IEEE Access
Multidisciplinary | Rapid Review | Open Access Journal

Received 22 June 2022, accepted 7 July 2022, date of publication 13 July 2022, date of current version 22 July 2022.

Digital Object Identifier 10.1109/ACCESS.2022.3190606

RESEARCH ARTICLE

Application of Near-Field Scanning Microwave Microscopy in Liquid Environment

YUJIE CHEN[1], XIANGYUE YANG[1], ZIQIAN WEI[1], HAN LUO[1], ZHIWEI YUAN[1], GUANXI JIANG[1], YAHUI WANG[1], AMIN UL HAQ[2], AND ZHE WU[3]

[1]Glasgow College, University of Electronic Science and Technology of China, Chengdu 611731, China
[2]School of Computer Science and Engineering, University of Electronic Science and Technology of China, Chengdu 611731, China
[3]School of Physics, University of Electronic Science and Technology of China, Chengdu 611731, China

Corresponding author: Zhe Wu (zhewu@uestc.edu.cn)

This work was supported in part by the Science and Technology Department of Sichuan Province under Grant 2020YJ0266, and in part by the College Students Innovative Entrepreneurial Training for the University of Electronic Science and Technology of China under Grant 202110614619 and Grant 202210614261X.

ABSTRACT In this article, a method of illustrating the electromagnetic properties of liquid specimens is proposed by our homemade near-field scanning microwave microscopy (NSMM). By introducing the fundamental theorem of NSMM and conducting a simulation on the configuration of the whole system, parameters including quality factor and resonant frequency in electrolyte liquid specimen vary with types of the solution as well as their concentration. By conducting the line scanning testing method, the relation of concentration of a specified solution concerning its corresponding electromagnetic properties is clarified. Eventually, yeast cells are tested at living or dead status with point scanning and line scanning separately. The NSMM experiment results exhibit a substantial capacity for biologic samples in a liquid environment.

INDEX TERMS Near-field microwave, electrolyte solution, yeast cells.

I. INTRODUCTION

With the development in the physic, chemistry, electronics, and biology field, there is a need to research the microscopic world. Different from the optical characterization, electromagnetic properties can also be discovered, avoiding the Abbe diffraction limit. That limits disable the optical microscope's resolution to explore the nano-range object. In 1928 and 1962, Synge and Soohoo demonstrated a method to utilize the microwave to interact with the complex permittivity, and the local conductivity of the specimen can also be deduced [1]–[3]. The technology of scanning microwave microscopy (SMM) has a breakthrough [4], and so has the NSMM system, which has already been explored with the potential to electronic industries [5], [6].

In microelectronic systems, the NSMM system also can be used in the application of carbon nanotube identification [5], buried conducting structure [7], [8], measuring the permittivity and loss of high-loss materials [9], and is also a common way to image two-dimensional device characterization [5], [6]. The research on bulk semiconductors about capacitance spectroscopy calibration and dopant profiling measurements indicated the potential application of NSMM in the analysis of property and failure in semiconductor devices [10]. The experiments on two-dimensional materials like GaN and other relevant devices [11]–[13] underscore that NSMM is capable to image the structure of materials and identifying structural defects. The phenomenon including microscopic phase separation and metal-insulator phase transitions about phase-change materials [14], [15] is also observed by NSMM.

Since microwave detection has a relatively higher sensitivity and the properties of non-destructive detection, it is appealing to the field of electrochemistry [16]–[18], biological [19]–[21], food industries, and medical industries [22], [23]. Especially in the study of medical imaging, it has attracted great interest during the past twenty years, since it has a significant capacity for the detecting abnormal tissue of the human body like malignant tissue, and the frequencies range of the electromagnetic is around 500 MHz to 10 GHz [24]–[28]. In 2004, Kim *et al.* [8] and other

The associate editor coordinating the review of this manuscript and approving it for publication was Giovanni Angiulli.

researchers successfully exploited NSMM fitted with the hybrid tip to obtain high contrast image of lambda phage DNA. The result indicated that NSMM using a hybrid tip has the potential to perform high contrast images for low sensitive and uneven materials. In 2012, Farina *et al.* [20] and his research team explored the structure of C_2Cl_2 muscle cells combined with multi-walled carbon nanotubes by utilizing the tomographic capability of NSMM. The outcome imaging highlighted the incorporation of carbon nanotubes into fibres grown inside muscle cells, which indicated the possibility of applying NSMM in tomographic imaging of cells. In 2016, time-gated broad NSMM was applied to detect fullerene inside breast cancer cells by measuring relevant electromagnetic quantities across the cells' surface [29]. The experimental results showed the reduction of microwave reflection, SCM signal contrast and the increase of surface roughness about fullerene treated cancer cells. This research sheds new light on the correlation between fullerene contented in cells and microwave imaging. And a typical environment for these industries is that the liquid environment is inevitable. In this scenario, the non-invading imaging method is essential to a certain degree, and the response of the electrolyte is needed further study. The following content focus on the experiment of the liquid specimen, other investigations about the yeast cell is illustrated in this article as well.

In this paper, we present further research about the application for the liquid environment, especially for KCl solution which is a common biological-related solution by near-field microwave microscopy. Analysis for the quality factor (Q) and central resonating frequency (f_r) for KCl specimen in the capillary are finished by line scanning. Finally, the yeast cell specimen is tested and verified, which can verify the substantial application of our homemade system in the field of biology and medical industries. The remaining section of the paper is organized as follows: In section II, methodology of the proposed model is discussed in detail, experiments are conducted and analyzed in section III, and section IV is the conclusion.

II. METHODS AND ANALYSIS

A. THEORETICAL BACKGROUND

The crucial part of the system is the perturbation method, which clarifies that the resonation properties could be interfered with by the vicinity environment.

For a specific resonator which in our configuration is made of copper and is a cylindrical co-axial resonator, together with the tips, parameters like v_0 (Volume) ε_0 (Permittivity) μ_0 (Permeability) E_0 (Electric field intensity) H_0 (magnetic field intensity) ω_0 (central resonating angular velocity) are determined. When a tested sample is placed beneath the tip of the resonator, parameters of material one and material two results in the offset centre frequency of the resonator. According to the Maxwell equation and divergence theorem, the change of centre frequency is introduced as follows in (1), as shown at the bottom of the next page.

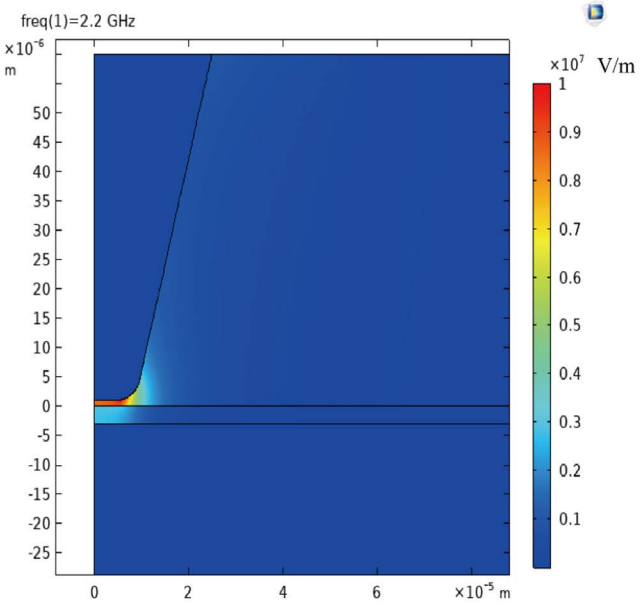

FIGURE 1. Simulated electric field distribution.

By comparing the specific parameters between the experimental group and the blank control group, minor disturbances caused by the specimen that would lead to errors can be analyzed separately, while combined with simulation, the electromagnetic properties can also be determined in value.

Since the specimen is in the type of liquid instead of the magnetic material, it can then be assumed that $\mu_1 = \mu_0$, as shown in (2).

$$\frac{\omega - \omega_s}{\omega_s} = \frac{\int_{v1} \left[\boldsymbol{E_1 E_0^*} \left(\varepsilon_1 - \varepsilon_0\right)\right] dv}{\int_{v1} \left(\boldsymbol{H_0 H_0^*} \mu_0 + \boldsymbol{E_0 E_0^*} \varepsilon_0\right) dv} \tag{2}$$

Therefore, it can be assumed that the change of the resonation frequency can have a linear relationship with the permittivity of the specimen, so as the power loss of the equivalent resistance for the whole system. When the conductivity of the specimen increases linearly, the reciprocal of Q could also increase concerning the conductivity. The E_{store} is the energy stored in the resonator, and Q is the quality factor that can be captured by the VNA and expressed in (3).

$$Q = \omega \frac{E_{total}}{P_{loss}} \tag{3}$$

As for simulation, COMSOL^{TM} is used as the software, which is a multi-physics field simulation software. The model in the research of the NSMM system of the COMSOL is composed of four parts, the tips of the resonator, the air medium, the glass plate, and the specimen under test, which is shown in Fig.1, illustrating the electric field distribution, indicating that the electric field exists in the vicinity of the apex. The narrower the tip is, the more concentrated the electric field of the tip will be. That is also the reason why when a higher resolution is required, the tip needs to be tinier, and the size of the tip should be larger, then the result could be relatively stable. It can also be found that the electric field can penetrate

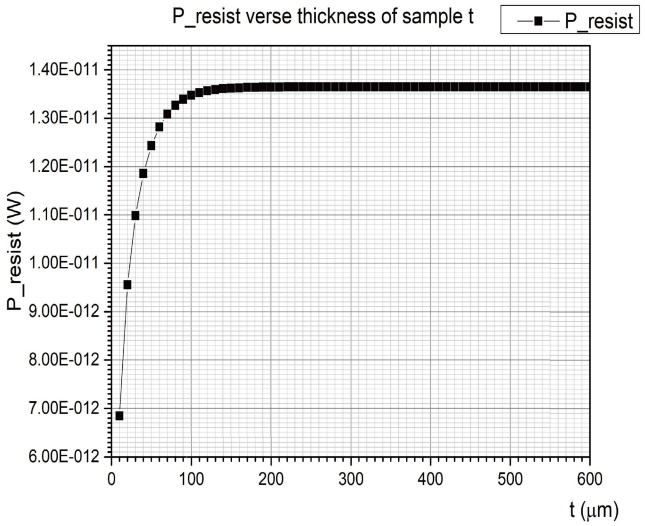

FIGURE 2. Power loss results from different tip-sample distances.

the capsulation of the specimen, enabling non-destructive detection of certain specimens, like the microfluidic chip or other biological specimens. Since electric field characteristics for various samples can be simulated through parameter scanning, physical quantities associated with and Q of cavity resonator f_r can be predicted according to simulation results. This beforehand simulation is practical for further research on the electric properties of liquid samples when a vector network analyzer is utilized to detect physical quantities.

Further exploration of other properties of the NSMM system is exhibited in Fig. 2. P_{loss} is composed of serval parts of the system, which can be illustrated in (4).

$$P_{loss} = P_{cav} + P_{tip} + P_{resist} \tag{4}$$

where P_{cav} is the power loss in the resonant cavity walls (which can be omitted), P_{tip} is power loss in the form of radiation due to tip-sample interaction, and P_{resist} is power loss due to the resistive heating of the sample in the simulation, $P_{loss} = P_{tip} + P_{resist}$ since P_{cav} is relatively small which can be omitted.

It is reasonable to infer the relationship between the P_{loss} for tip-sample distance and the thickness of the liquid specimen. It suggests that when the thickness of the common liquid sample t is over 200 μm, the scanning microwave generated by the VNA can be absorbed totally, and no more electromagnetic properties beneath the specimen could be discovered. As for the gap between the tip sample distance, it is found that for an apex with a radius of 50 μm, the range of space that the probe can detect is about 100 μm. With a larger size, the electric field will be less concentrated, and the detection range for the tips will be wider.

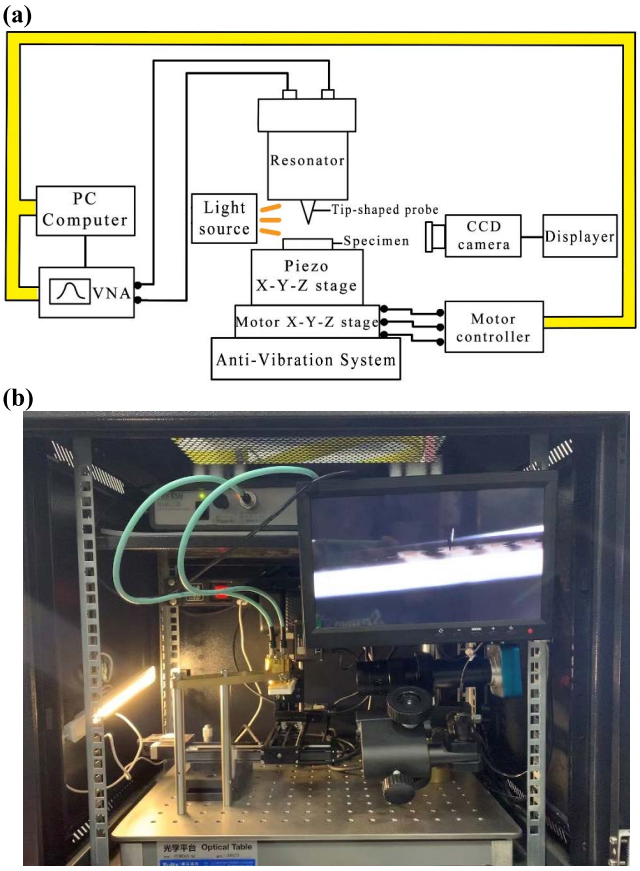

FIGURE 3. Schematic and (b) photo of the NSMM experimental setup.

B. EXPERIMENTAL CONFIGURATION

The NSMM experimental setup shown in Fig. 3 (a) and Fig. 3 (b) is composed of four parts. A charge-coupled device (CCD) camera with a displayer, structure and control system, resonator combined with a tip-shaped probe, and a Vector Network Analyzer (VNA).

The CCD with a displayer is used to monitor the tip-sample distance and the position of the probe, indicating to what extent the motor stage can be adjusted. The structure and control system are set up as a platform to carry out the experiment, which covers a bracket (to fix the resonant tank), an x-y-z motor stage, an air cushion vibration isolation optical table and the manipulated laptop (to control the movement of the motor stage through LabView^{TM}2018). The chosen resonator is a $\lambda/4$ coaxial gliding one connected with a hyperfine copper probe with a size of about 10μm. Compared with other types of resonators like planar resonators [31], [32], our homemade $\lambda/4$ coaxial cylindrical resonator together with x-y-z motor stage shows the ability to obtain three-dimensional images of electromagnetic properties of

$$\frac{\omega - \omega_s}{\omega_s} = \frac{\int_{v1} \left[\mathbf{E_1 E_0^*} (\varepsilon_1 - \varepsilon_0) + \mathbf{H_1 H_0^*} (\mu_1 - \mu_0)\right] dv}{\int_{v1} \left(\boldsymbol{H_1 H_0^*} \mu_0 + \boldsymbol{E_1 E_0^*} \varepsilon_0\right) dv + \int_{v1} \left(\boldsymbol{H_2 H_0^*} \mu_0 + \boldsymbol{E_2 E_0^*} \varepsilon_0\right) dv} \tag{1}$$

TABLE 1. Comparation among different resonators.

Setup	NSMM	Planar Reflective Sensor [31]	Planar Microwave Sensor [32]
Description	Coaxial cylindrical resonator	Complementary split ring resonator	Metamaterial planar sensor
Frequency	2.0 - 2.5 GHz	2.0 – 3.0 GHz	5.0 – 7.0 GHz
Advance	Imaging, 2μm spatial resolution [30]	High sensitivity	High sensitivity

the specimen with higher resolution. Its spatial resolution can achieve 2 μm [30]. The specific comparation among them is shown in Table 1.

Through the lines, the resonator is connected to a vector network analyzer (VNA, Agilent Technologies E5062A).

To explore the NSMM on liquid, scanning samples are required to be determined as well.

Before the beginning of the experiment, the specimen was prepared. Deionized water with a volume of 100mL is taken to prepare the solution in a specific concentration are held in a 10.0 × 10.0 × 1.0 mm groove to do the scanning. With the deionized water acting as a blank control, $MgCl_2$, $CaCl_2$ and KCl solutions are chosen as the target scanning samples, because K^+, Mg^{2+} and Ca^{2+} cover most of the positive ions' percentage in the cell gap. Their detailed concentrations of them are shown in the attachment. Since the previous study has already conducted research about NSMM on plant scanning as the leaves, therefore, a typical and common biological material-yeast cell is introduced in the further experiment in our study.

There are several types of scanning methods in our NSMM setup: point scanning, line scanning and so on. Examples of those three methods are shown in Fig. 4 (a)-(c).

For point scanning, the first step is that stage goes up and down in z-direction but fixed at a specific x-y position, and then the response changes that would be detected by VNA as the tip-sample distance varies, which can also be indicated by the simulation result from Fig. 2. As it can be seen in Fig. 5 (a)-(c), initially, when the probe tip gradually approaches the specimen, a relatively stable quality factor Q can be observed even the distance changes, and this is called soft contact. During the point scanning, the soft contact is essential for the point scanning because the Q and other parameters obtained by the VNA would be vastly influenced by the tip-sample distance. The main purpose of defining the soft contact is to make sure that the tip-sample distance is fixed while the coordinate recorded by the piezo x-y-z motor stage is varying so that when the tip leaves the specimen the tip-sample distance can still be identified by subtracting the coordinate of 'turning point' from the recorded coordinate of the indicated point. During this stage, a moderate vertical movement of the stage in height will cause no change to the sample's response because the spring inside the resonator can be pressed. Finally, the experimental result is obtained and analyzed.

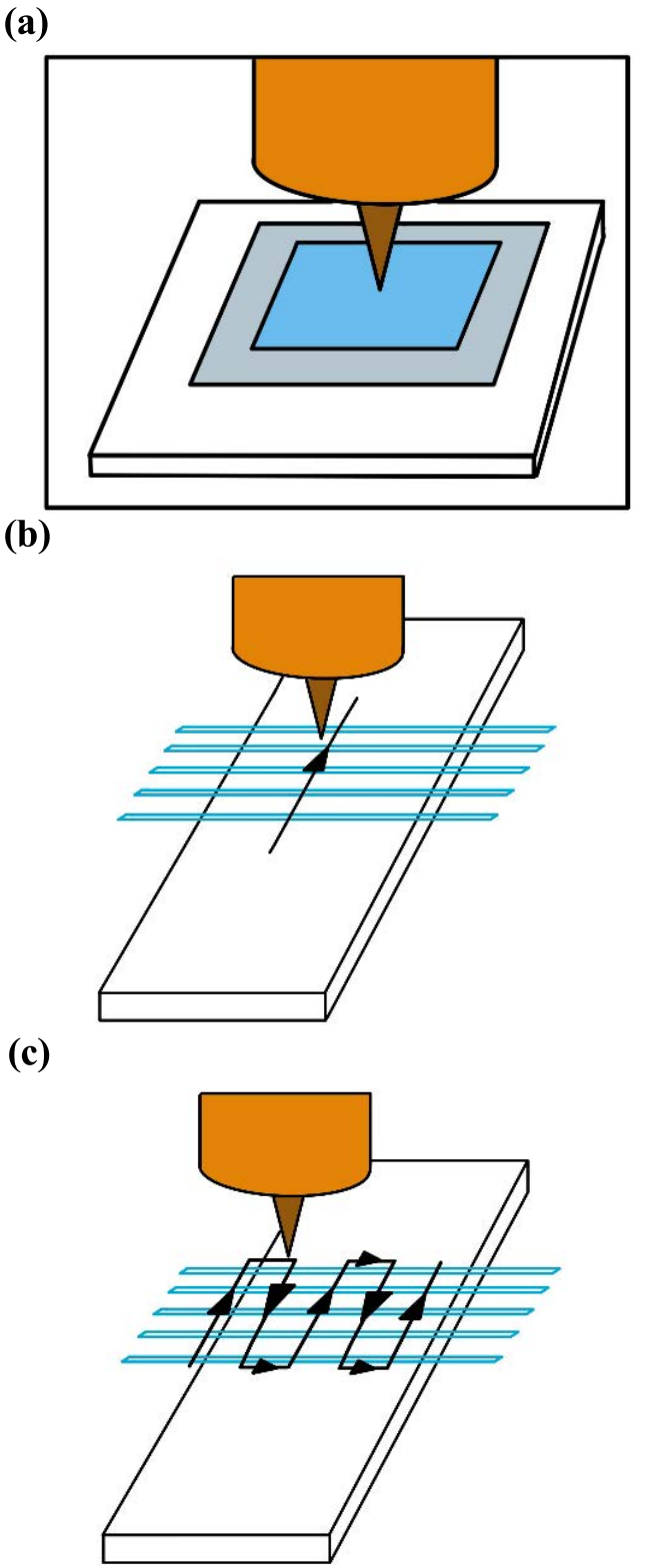

FIGURE 4. Scanning process includes (a) point scanning, (b) line scanning and (c) surface scanning.

For line scanning, the motor stage is fixed in the z-direction, and then the response information alone x or y direction (a line) is collected.

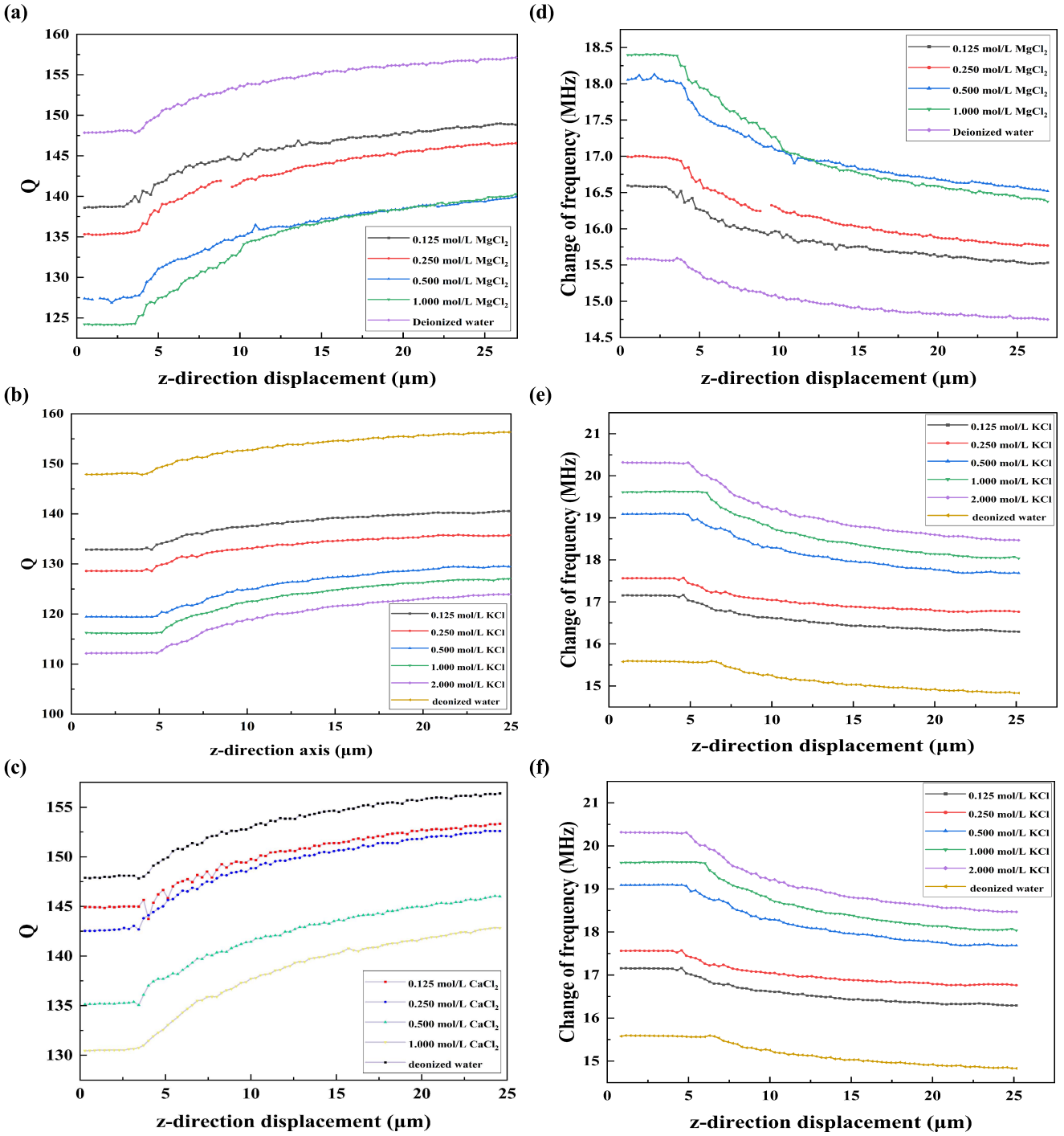

FIGURE 5. Results of the point scanning. Change of Q versus z-direction displacement when the testing liquid is (a) $MgCl_2$, (b) KCl and (c) $CaCl_2$. Change of f_r versus z-direction displacement when the testing liquid is (d) $MgCl_2$, (e) KCl and (f) $CaCl_2$.

III. RESULTS AND ANALYSIS

In the first stage, we did the point scanning on $MgCl_2$, KCl and $CaCl_2$ solution of 4 or 5 increasing concentrations, whose value is from 0.0 mol/L (deionized water) to 1.0 mol/L or 2.0 mol/L, and the response including the quality factor (Q) and the bias of the resonator frequency (f_r) to tip-sample distances were collected as shown in Fig. 5 (a)-(f). Generally, the distance for soft contact is from 0 μm to around 5 μm, and the values of Q and f_r are affected by the types of the solution as well as the concentrations of the solution. It demonstrates that Q would increase as the tip-sample distance increases as the concentration remains fixed, or the concentration decreases as the tip-sample distance remains invariant. On the contrary, f_r decreases either for the increasing tip-sample distance or

the decreasing concentration. In the aspect of the types of the solution, $MgCl_2$ and $CaCl_2$ have a relatively closer value of Q and f_r compared with KCl, probably because Mg^{2+} and Ca^{2+} are both divalent cations and have similar features.

Results of the point scanning. Change of Q versus z-direction displacement when the testing liquid is (a) $MgCl_2$, (b) KCl and (c) $CaCl_2$. Change of f_r versus z-direction displacement when the testing liquid is (d) $MgCl_2$, (e) KCl and (f) $CaCl_2$.

It can be concluded that NSMM is sensible to detect electromagnetic discrepancies of different types and molarities of saline-solution specimens under a coverslip. To be more specific, both Q curves and f_r curves differ in various solutions and various concentrations of a given solution because factors such as conductivity and permittivity are different.

In the second stage, the probe tip is placed at a fixed distance above the KCl solution sample to do the line scanning. Fig. 5 (a) - (c) is a curve of the scanning result-quality factor (Q) and Fig. 5 (d) - (f) is the change of the resonator frequency (Δf_r) for serval different types of solutions in different molarities. The central resonate frequency with the specimen compared with its no-load state. The frequency variation can help adjust the tip-sample distance to an appropriate distance [30], and it has potential application in other soft materials like biological cells [33]. Each concave in these figures represents the samples of specific molarities as solutions of different molarities have different electromagnetic parameters. It is shown that the higher concentrations are, the stronger the conductive ability it will have, and the more power dissipation would produce by the total equivalent resistance, then the lower Q VNA could acquire. However, there is no obvious variety regulation for f_r as the concentration varies in decreasing order. After extracting concaves from line-scanning graphs of KCl in a fixed concentration gradient, Q is exhibited in Fig. 6 (c). By presenting the processed sunken range of Q, this graph illustrates that higher concentration would lead to smaller values of Q. Thus, the same solutions in different concentrations could be recognized. To better visualize this regularity, Fig. 6 (d) that shows the change ratio of both Q and f_r is plotted, which is calculated by $(Q_0 - Q)/Q_0$ and $(f_{r0} - f_r')/f_{r0}$, where Q_0 and f_{r0} are the corresponding parameters of the resonator itself, and this value has a strong relationship with permittivity. Q and f_r' are the measured result for Q and resonant frequency. Q grows linearly by the rise of the concentration while there is only slight or even no increment of f_r as the concentration increases.

As K^+ is one of the most common ions existing in the cell sap, the previous experimental result is therefore extended to the biological specimen, the yeast cells. There are two kinds of the specimen, the living yeast cell in its corresponding nutrient solution, as for reference, another group is processed at high temperature to make sure its death. In the experiment results shown in Fig. 7 (a) and (b), the living yeast cell is condensed under the covering glass (0.1mm), enabling us to make sure that there will always be living yeast cells directly under the tips, and another specimen is the dead yeast cells.

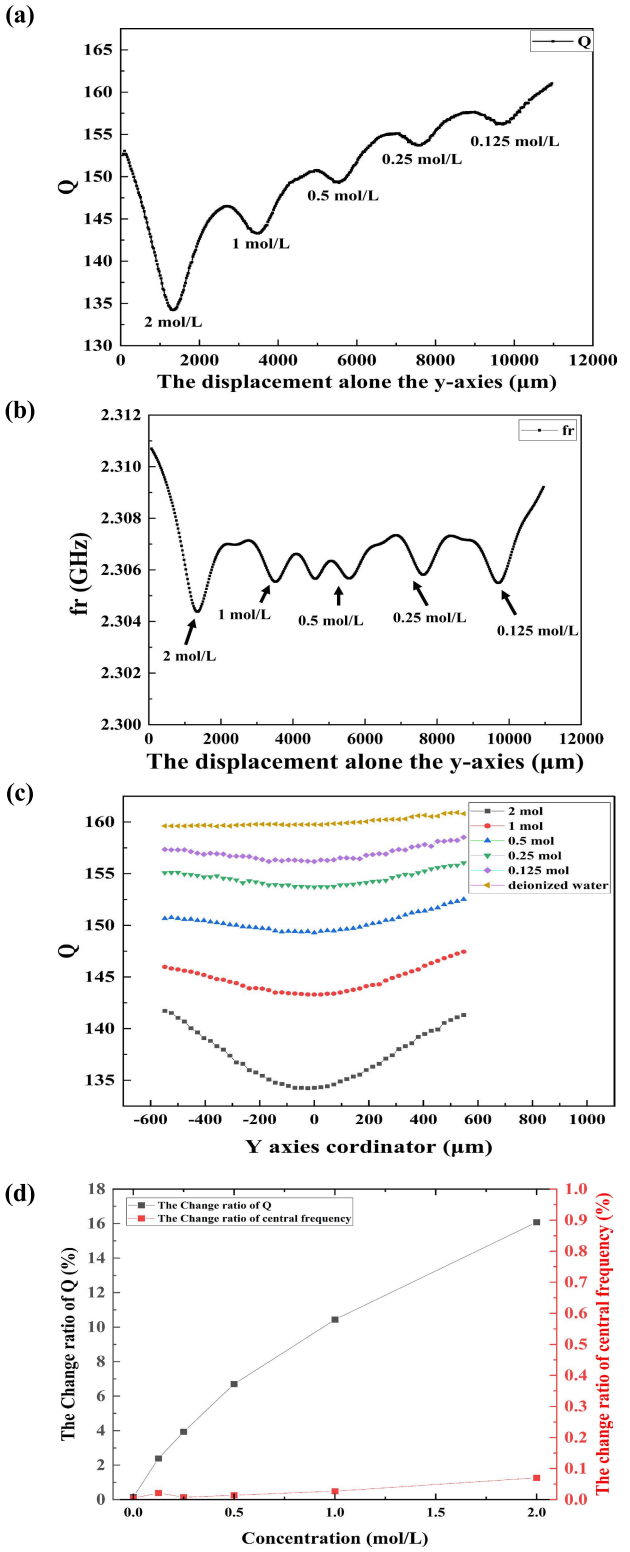

FIGURE 6. Results of the line scanning. (a) Change of Q for KCl. (b) Change of f_r for KCl. (c) Change of Q with different concentrations. (d) Compared rate of Q and f_r versus concentration of the tested sample.

The Q result is illustrated in Fig. 7 (a), which demonstrates that there is slight but distinguished Q curves for the yeast cell and the reference group. And from this graph, it could also be found that the imaging of the yeast cell must be close

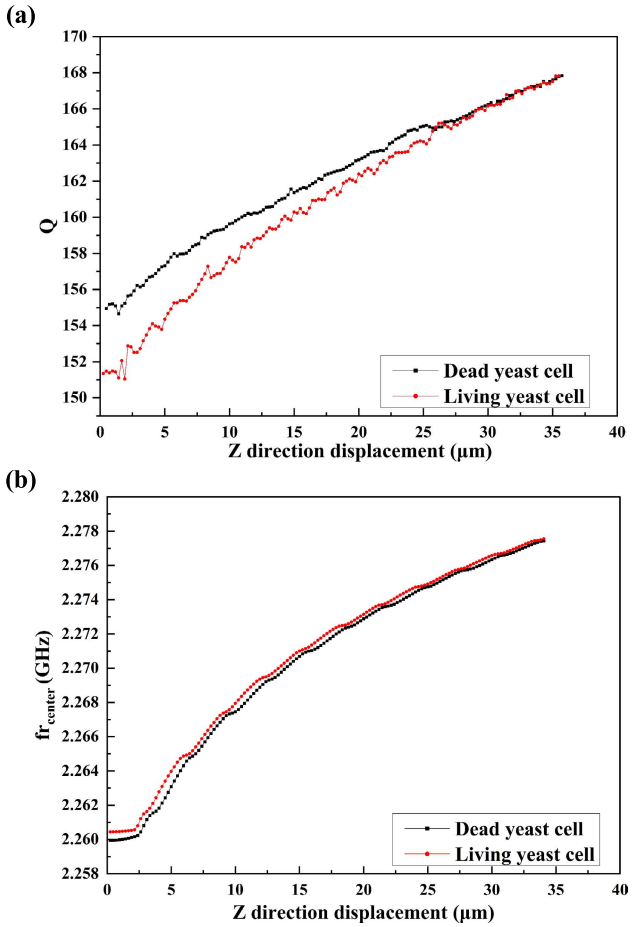

FIGURE 7. Results of yeast cell scanning. Difference of (a) Q and (b) f_r versus Z-direction displacement between specimens with alive and dead yeast cells.

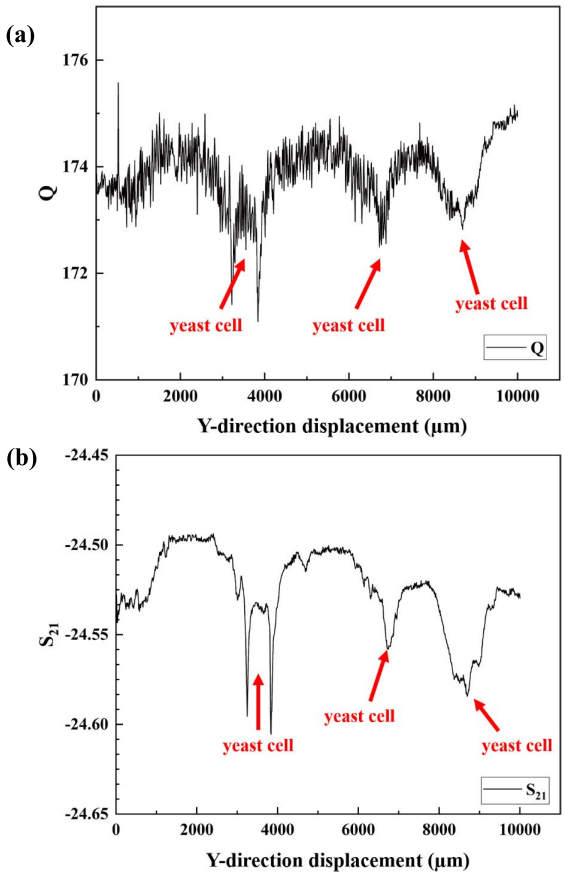

FIGURE 8. Scanning results on yeast cells with evenly distributed gaps. Difference about (a) Q and (b) S_{21}.

enough to the specimen, especially when there is a covering material like silica glass. The different Q also illustrates the penetrating ability of our system that helps to do further research on the encapsulated microfluidic chips, as it also has a covering material. However, as indicated in Fig. 7 (b), the central resonating frequency can hardly be distinguished, therefore, the further experiment for these kinds of biological material had better focus on the quality factor or the phase angle collected by the VNA.

To further research on the Q and f_r of yeast and do the comparison with the no-load test, line scanning is carried out with evenly distributed gaps among groups of yeasts on the glass slide, with the result shown in Fig. 8. During this process, the dried yeasts are set on the glass slide, with several no-load lines evenly distributed. As discussed above, the Q of yeast is lower than that of air (no load), thus, in Fig. 8, there are several bulges of Q-value and S_{21}-value, representing the no-load area. f_r curve is not plotted because Fig. 7 (b) demonstrates that there is no evident difference between the yeast and the no-load sample. Fig. 8 (a) and Fig. 8 (b) have a similar varying tendency, but it is obvious that Fig. 8 (a) has more noise, indicating that SNR of Q is lower than that of S_{21}, therefore, S_{21} could better act as the distinguishing method. With these periodic waves detected by the VNA, the conclusion could be drawn that signals are successfully extracted.

IV. CONCLUSION

In conclusion, further research about the non-destructive, non-invasive and penetrative properties is illustrated by the experiment of the KCl specimen held in the capillaries. The electrolyte liquid specimen in the micro-pipe system is tested with line scanning which can prepare for NSMM imaging of the microfluidic chip specimen. Finally, we apply the NSMM system to biological specimens, with different statuses of living or death and the potential capability of our system to test the related properties of the biological material, which might be the fundamental for the further experiment for the single-cell detection or research of the imaging for the microfluidic chips.

ACKNOWLEDGMENT

(Yujie Chen and Xiangyue Yang are co-first authors.)

REFERENCES

[1] E. H. Synge, "XXXVIII. A suggested method for extending microscopic resolution into the ultra-microscopic region," *London, Edinburgh, Dublin Phil. Mag. J. Sci.*, vol. 6, no. 35, pp. 356–362, Aug. 1928, doi: 10.1080/14786440808564615.

[2] R. F. Soohoo, "A microwave magnetic microscope," *J. Appl. Phys.*, vol. AP-33, no. 3, p. 1276, 1962, doi: 10.1063/1.1728690.
[3] A. Gregory, L. Hao, N. Klein, J. Gallop, C. Mattevi, O. Shaforost, K. Lees, and B. Clarke, "Spatially resolved electrical characterisation of graphene layers by an evanescent field microwave microscope," *Phys. E, Low-Dimensional Syst. Nanostruct.*, vol. 56, pp. 431–434, Feb. 2014, doi: 10.1016/J.PHYSE.2012.10.006.
[4] M. Farina and J. C. M. Hwang, "Scanning microwave microscopy for biological applications: Introducing the state of the art and inverted SMM," *IEEE Microw. Mag.*, vol. 21, no. 10, pp. 52–59, Oct. 2020, doi: 10.1109/MMM.2020.3008239.
[5] G. Georg, K. Alexander, L. Tingbin, J. Z. S. Taylor, S. Hari, R. S. Steven, B. Enrico, A. Gabriel, K. Ferry, and J. C. Neil, "Nondestructive imaging of atomically thin nanostructures buried in silicon," *Sci. Adv.*, vol. 3, no. 6, May 2022, Art. no. e1602586, doi: 10.1126/sciadv.1602586.
[6] J. C. Weber, P. T. Blanchard, and A. W. Sanders, "Gallium nitride nanowire probe for near-field scanning microwave microscopy," *Appl. Phys. Lett.*, vol. 104, no. 2, 2014, Art. no. 113701, doi: 10.1063/1.4861862.
[7] A. Javey, J. Guo, Q. Wang, M. Lundstrom, and H. Dai, "Ballistic carbon nanotube field-effect transistors," *Nature*, vol. 424, pp. 654–657, Aug. 2003, doi: 10.1038/nature01797.
[8] M. Kim, J. Kim, H. Kim, S. Kim, J. Yang, H. Yoo, S. Kim, and K. Lee, "Nondestructive high spatial resolution imaging with a 60 GHz near-field scanning millimeter-wave microscope," *Rev. Sci. Instrum.*, vol. 75, no. 3, p. 684, 2004, doi: 10.1063/1.1646735.
[9] A. P. Gregory, J. F. Blackburn, K. Lees, R. N. Clarke, T. E. Hodgetts, S. M. Hanham, and N. Klein, "A near-field scanning microwave microscope for measurement of the permittivity and loss of high-loss materials," in *Proc. 84th ARFTG Microw. Meas. Conf.*, Dec. 2014, pp. 1–8, doi: 10.1109/ARFTG.2014.7013419.
[10] H. P. Huber, I. Humer, M. Hochleitner, M. Fenner, M. Moertelmaier, C. Rankl, A. Imtiaz, T. M. Wallis, H. Tanbakuchi, P. Hinterdorfer, P. Kabos, J. Smoliner, J. J. Kopanski, and F. Kienberger, "Calibrated nanoscale dopant profiling using a scanning microwave microscope," *J. Appl. Phys.*, vol. 111, no. 1, p. 14301, 2012, doi: 10.1063/1.3672445.
[11] S. Berweger, J. C. Weber, J. John, J. M. Velazquez, A. Pieterick, N. A. Sanford, A. V. Davydov, B. Brunschwig, N. S. Lewis, T. M. Wallis, and P. Kabos, "Microwave near-field imaging of two-dimensional semiconductors," *Nano Lett.*, vol. 15, no. 2, pp. 1122–1127, Feb. 2015, doi: 10.1021/nl504960u.
[12] S. Berweger, P. T. Blanchard, and M. D. Brubaker, "Near-field control and imaging of free chargecarrier variations in GaN nanowires," *Appl. Phys. Lett.*, vol. 108, p. 73101, Feb. 2016, doi: 10.1063/1.4942107.
[13] W. Choi, E. Seabron, P. K. Mohseni, J. D. Kim, T. Gokus, A. Cernescu, P. Pochet, H. T. Johnson, W. L. Wilson, and X. Li, "Direct electrical probing of periodic modulation of zinc-dopant distributions in planar gallium arsenide nanowires," *ACS Nano*, vol. 11, p. 18, Jan. 2017, doi: 10.1021/acsnano.6b06853.
[14] A. Tselev, V. Meunier, E. Strelcov, W. A. Shelton, I. A. Luk'yanchuk, K. Jones, R. Proksch, A. Kolmakov, and S. V. Kalinin, "Mesoscopic metalinsulator transition at ferroelastic domain walls in VO_2," *Acs Nano*, vol. 48, p. 39, Jul. 2022, doi: 10.1021/nn1004364.
[15] L. Keji, N. Masao, K. Worasom, K. Masashi, T. Yoshinori, K. A. Michael, and S. Zhixun, "Mesoscopic percolating resistance network in a strained manganite thin film," *Science*, vol. 329, no. 5988, pp. 190–193, Jul. 2010, doi: 10.1126/science.1189925.
[16] M. Saadat-Safa, V. Nayyeri, A. Ghadimi, M. Soleimani, and O. M. Ramahi, "A pixelated microwave near-field sensor for precise characterization of dielectric materials," *Sci. Rep.*, vol. 9, no. 1, pp. 1–12, Dec. 2019, doi: 10.1038/s41598-019-49767-w.
[17] S. Grall, I. Alic, E. Pavoni, M. Awadein, T. Fujii, S. Müllegger, M. Farina, N. Clement, and G. Gramse, "Attoampere nanoelectrochemistry," *Small*, vol. 17, no. 29, Jul. 2021, Art. no. 2101253, doi: 10.1002/smll.202101253.
[18] S. Gu, T. Lin, and T. Lasri, "Dielectric properties characterization of saline solutions by near-field microwave microscopy," *Meas. Sci. Technol.*, vol. 28, no. 1, Jan. 2017, Art. no. 014014, doi: 10.1088/1361-6501/28/1/014014.
[19] Y. Wang, Z. Wei, Y. Chen, Q. Zhou, Y. Gong, B. Zeng, and Z. Wu, "An approach to determine solution properties in micro pipes by near-field microwave microscopy," *J. Phys., Condens. Matter*, vol. 34, no. 5, Feb. 2022, Art. no. 054001, doi: 10.1088/1361-648X/ac3308.
[20] M. Farina, A. Di Donato, T. Monti, T. Pietrangelo, T. Da Ros, A. Turco, G. Venanzoni, and A. Morini, "Tomographic effects of near-field microwave microscopy in the investigation of muscle cells interacting with multi-walled carbon nanotubes," *Appl. Phys. Lett.*, vol. 101, no. 20, Nov. 2012, Art. no. 203101, doi: 10.1063/1.4767518.
[21] F. Kazemi, F. Mohanna, and J. Ahmadi-Shokouh, "Microwave near-field imaging of biological samples using a microstrip resonator probe," *IETE J. Res.*, vol. 66, no. 5, pp. 600–607, Sep. 2020, doi: 10.1080/03772063.2018.1510745.
[22] W. Shao and T. McCollough, "Advances in microwave near-field imaging: Prototypes, systems, and applications," *IEEE Microw. Mag.*, vol. 21, no. 5, pp. 94–119, May 2020, doi: 10.1109/MMM.2020.2971375.
[23] C.-H. Tseng, T.-J. Tseng, and C.-Z. Wu, "Cuffless blood pressure measurement using a microwave near-field self-injection-locked wrist pulse sensor," *IEEE Trans. Microw. Theory Techn.*, vol. 68, no. 11, pp. 4865–4874, Nov. 2020, doi: 10.1109/TMTT.2020.3011446.
[24] K. L. Carr, P. Cevasco, P. Dunlea, and J. Shaeffer, "Radiometric sensing: An adjuvant to mammography to determine breast biopsy," in *IEEE MTT-S Int. Microw. Symp. Dig.*, vol. 2, Jan. 2000, pp. 929–932, doi: 10.1109/MWSYM.2000.863509.
[25] P. M. Meaney, M. W. Fanning, D. Li, S. P. Poplack, and K. D. Paulsen, "A clinical prototype for active microwave imaging of the breast," *IEEE Trans. Microw. Theory Techn.*, vol. 48, no. 11, pp. 1841–1853, Nov. 2000, doi: 10.1109/22.883861.
[26] E. C. Fear, S. C. Hagness, P. M. Meaney, M. Okoniewski, and M. A. Stuchly, "Enhancing breast tumor detection with near-field imaging," *IEEE Microw. Mag.*, vol. 3, no. 1, pp. 48–56, Mar. 2002, doi: 10.1109/6668.990683.
[27] N. K. Nikolova, "Microwave imaging for breast cancer," *IEEE Microw. Mag.*, vol. 12, no. 7, pp. 78–94, Dec. 2011, doi: 10.1109/MMM.2011.942702.
[28] A. Fhager, S. Candefjord, M. Elam, and M. Persson, "Microwave diagnostics ahead: Saving time and the lives of trauma and stroke patients," *IEEE Microw. Mag.*, vol. 19, no. 3, pp. 78–90, May 2018, doi: 10.1109/MMM.2018.2801646.
[29] M. Farina, F. Piacenza, F. D. Angelis, D. Mencarelli, A. Morini, G. Venanzoni, T. Pietrangelo, M. Malavolta, A. Basso, M. Provinciali, and J. C. M. Hwang, "Investigation of fullerene exposure of breast cancer cells by time-gated scanning microwave microscopy," *IEEE Trans. Microw. Theory Techn.*, vol. 64, no. 12, pp. 4823–4831, Dec. 2016, doi: 10.1109/TMTT.2016.2623312.
[30] X. Zhang, Z. Wu, Q. Lan, Z. Du, Q. Zhou, R. Jiang, J. Liu, Y. Gong, and B. Zeng, "Improvement of spatial resolution by tilt correction in near-field scanning microwave microscopy," *AIP Adv.*, vol. 11, no. 1, p. 35114, Mar. 2021, doi: 10.1063/5.0045355.
[31] N. Kazemi, K. Schofield, and P. Musilek, "A high-resolution reflective microwave planar sensor for sensing of vanadium electrolyte," *Sensors*, vol. 21, no. 11, p. 3759, May 2021, doi: 10.3390/s21113759.
[32] M. Abdolrazzaghi, M. Daneshmand, and A. K. Iyer, "Strongly enhanced sensitivity in planar microwave sensors based on metamaterial coupling," *IEEE Trans. Microw. Theory Techn.*, vol. 66, no. 4, pp. 1843–1855, Apr. 2018, doi: 10.1109/TMTT.2018.2791942.
[33] Z. Wu, W.-Q. Sun, T. Feng, S. W. Tang, G. Li, K.-L. Jiang, S.-Y. Xu, and C. K. Ong, "Imaging of soft material with carbon nanotube tip using near-field scanning microwave microscopy," *Ultramicroscopy*, vol. 148, pp. 75–80, Jan. 2015, doi: 10.1016/J.ULTRAMIC.2014.09.008.

YUJIE CHEN is currently pursuing the B.S. degree with the University of Electronic Science and Technology of China, Chengdu, China, and the B.Eng. degree with the University of Glasgow, Chengdu. Since 2020, he has been a member of Prof. Zhe Wu's Group and he currently plans to receive further M.S. education at the University of California, Los Angeles (UCLA), in October 2022. His research interests include physical and wave electronics like microwave, photonics, quantum electronics, and quantum repeater.

XIANGYUE YANG is currently pursuing the degree in electrical engineering with the University of Electronic Science and Technology of China. As a Junior Student, she has done some research on near-field microwave, blood pressure, and encryption communication, also presented at INFOCOM meeting, in 2022, focusing on authentication of Internet of Vehicles.

ZIQIAN WEI is currently pursuing the B.S. degree in electronics and electrical engineering from the University of Electronic Science and Technology of China (UESTC), Chengdu, China.

She has participated in summer school at the University of California, Los Angles, from June 2021 to September 2021. Since 2019, she has been a Research Assistant with Prof. Zhe Wu's Laboratory and Prof. Hao Fu's Laboratory. Her research interests include near-field scanning microwave microscopy for liquid, strong red upconversion luminescence and optical thermometry of nanomaterials, and low-temperature synthesis of nanoparticles with controlled crystal growth for efficient ultraviolet photocatalyst.

HAN LUO was born in Sichuan, China, in 2001. He is currently pursuing the bachelor's degree with the University of Electronic Science and Technology of China, Chengdu, China.

From 2020 to 2022, he has delivered an article as the second author at the 14th International Conference on Damage Assessment of Structure and drafted a patent in the field of microwave application.

ZHIWEI YUAN is currently pursuing the bachelor's degree in electronic and electrical engineering with the University of Electronic Science and Technology of China, Chengdu, Sichuan, China.

From 2021 to 2022, she is developing her interest in applied physics, especially for near-field microwave microscopy (NSMM). Her research interests include imaging micro-biological specimen using NSMM and developing methods for measuring flow velocities in varying types of microfluidics. She has participated at the program studying solution properties in micro pipes by near-field microwave microscopy, which was awarded the provincial project. In 2022, she was responsible for the program which explores microfluidics and delivered a patent of a novel method to measure flow velocities.

GUANXI JIANG is currently pursuing the bachelor's degree in electronics and electrical engineering with the joint program between the University of Electronic Science and Technology of China (UESTC) and the University of Glasgow (UoG). In the near future, he will pursue the master's degree in information technology with The Hong Kong University of Science and Technology (HKUST). His research interests include neuromorphic computing and machine learning, which enable himself to possess state-of-the-art technologies to improve the world.

YAHUI WANG received the B.Eng. degree in electrical and electronic engineering from the University of Electronic Science and Technology of China (UESTC), Chengdu, in 2022. Her research interests include near-field microwave microscopy and microwave imaging.

AMIN UL HAQ is currently working as a Postdoctoral Scientific Research Fellow with the University of Electronic Science and Technology of China (UESTC), China. He has a vast academic, technical, and professional experience at Pakistan. He is also a Lecturer with The University of Agricultural Peshawar, Pakistan. He is also associated with the Wavelets Active Media Technology and Big Data Laboratory as a Postdoctoral Scientific Research Fellow. He has published 27 SCI high-level research articles in good journals. His research interests include machine learning, deep learning, medical big data, the IoT, e-health and telemedicine, concerned technologies, and algorithms. He is an invited reviewer for numerous world-leading high-impact journals (reviewed more than 70 journal articles to date).

ZHE WU received the Ph.D. degree in physics from Nanjing University, in 2008. From 2012 to 2014, she was a Research Fellow at the National University of Singapore. She is currently a Professor with the School of Physics, University of Electronic Science and Technology of China. Her research interests include electromagnetic parametric measurements, electromagnetic field simulation, and application for microwave energy.